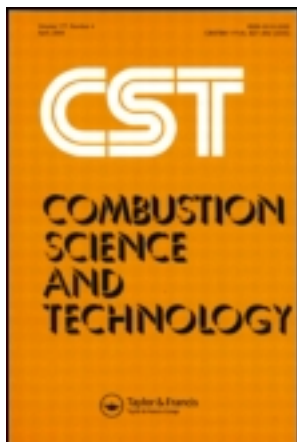


This article was downloaded by: [Indian Institute of Science], [Varunkumar Sivakumar]
On: 13 October 2011, At: 23:00
Publisher: Taylor & Francis
Informa Ltd Registered in England and Wales Registered Number: 1072954 Registered
office: Mortimer House, 37-41 Mortimer Street, London W1T 3JH, UK



Combustion Science and Technology

Publication details, including instructions for authors and
subscription information:

<http://www.tandfonline.com/loi/gcst20>

Single Particle and Packed Bed Combustion in Modern Gasifier Stoves—Density Effects

S. Varunkumar^a, N. K. S. Rajan^a & H. S. Mukunda^a

^a Combustion Gasification and Propulsion Laboratory, Department of
Aerospace Engineering, Indian Institute of Science, Bangalore, India

Available online: 03 Oct 2011

To cite this article: S. Varunkumar, N. K. S. Rajan & H. S. Mukunda (2011): Single Particle and Packed
Bed Combustion in Modern Gasifier Stoves—Density Effects, Combustion Science and Technology,
183:11, 1147-1163

To link to this article: <http://dx.doi.org/10.1080/00102202.2011.576658>

PLEASE SCROLL DOWN FOR ARTICLE

Full terms and conditions of use: <http://www.tandfonline.com/page/terms-and-conditions>

This article may be used for research, teaching, and private study purposes. Any
substantial or systematic reproduction, redistribution, reselling, loan, sub-licensing,
systematic supply, or distribution in any form to anyone is expressly forbidden.

The publisher does not give any warranty express or implied or make any representation
that the contents will be complete or accurate or up to date. The accuracy of any
instructions, formulae, and drug doses should be independently verified with primary
sources. The publisher shall not be liable for any loss, actions, claims, proceedings,
demand, or costs or damages whatsoever or howsoever caused arising directly or
indirectly in connection with or arising out of the use of this material.

SINGLE PARTICLE AND PACKED BED COMBUSTION IN MODERN GASIFIER STOVES—DENSITY EFFECTS

S. Varunkumar, N. K. S. Rajan, and H. S. Mukunda

Combustion Gasification and Propulsion Laboratory, Department of Aerospace Engineering, Indian Institute of Science, Bangalore, India

This article is concerned with a study of an unusual effect due to density of biomass pellets in modern stoves based on close-coupled gasification-combustion process. The two processes, namely, flaming with volatiles and glowing of the char show different effects. The mass flux of the fuel bears a constant ratio with the air flow rate of gasification during the flaming process and is independent of particle density; char glowing process shows a distinct effect of density. The bed temperatures also have similar features: during flaming, they are identical, but distinct in the char burn (gasification) regime. For the cases, wood char and pellet char, the densities are 350, 990 kg/m³, and the burn rates are 2.5 and 3.5 g/min with the bed temperatures being 1380 and 1502 K, respectively. A number of experiments on practical stoves showed wood char combustion rates of 2.5 ± 0.5 g/min and pellet char burn rates of 3.5 ± 0.5 g/min. In pursuit of the resolution of the differences, experimental data on single particle combustion for forced convection and ambient temperatures effects have been obtained. Single particle char combustion rate with air show a near- d^2 law and surface and core temperatures are identical for both wood and pellet char. A model based on diffusion controlled heat release—radiation—convection balance is set up. Explanation of the observed results needs to include the ash build-up over the char. This model is then used to explain observed behavior in the packed bed; the different packing densities of the biomass chars leading to different heat release rates per unit bed volume are deduced as the cause of the differences in burn rate and bed temperatures.

Keywords: Ash effect; Biomass gasifier stove; Char mode; Char particle combustion; Flaming mode

INTRODUCTION

The origin of the problem addressed here is related to a gasification-based stove design that the laboratory has been involved in over the last five years; specifically, a 3 kWth domestic stove was designed using gasification principles, and the design has recently been commercialized (Mukunda et al., 2010). This stove shown in Figure 1 has a combustion space of 100 mm diameter and 130 mm depth with a grate in the bottom, and wood chips or pellets of biomass can be used as fuel. Air for gasification (primary air) is provided from the bottom region, and the gas generated in the process of

Received 14 October 2010; revised 26 March 2011; accepted 28 March 2011.

Address correspondence to S. Varunkumar, Combustion Gasification and Propulsion Laboratory, Department of Aerospace Engineering, Indian Institute of Science, Bangalore, India. E-mail: varunsivakumar@gmail.com

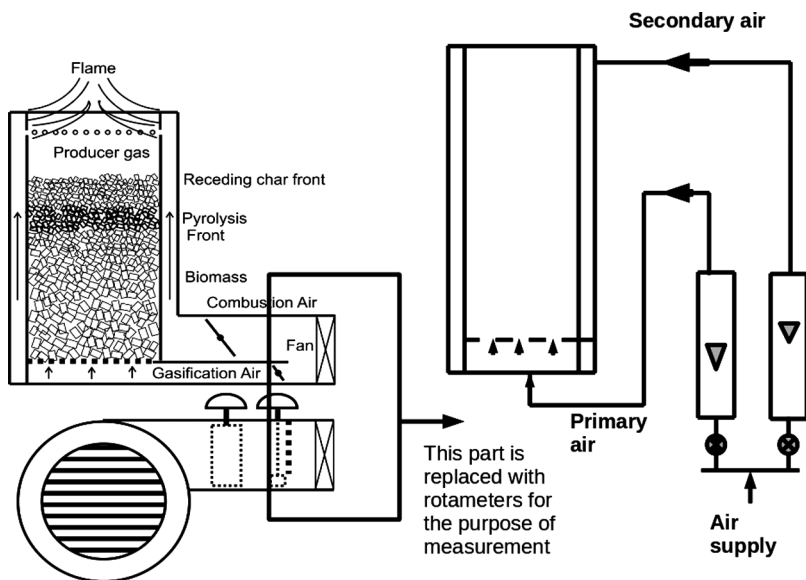


Figure 1 Schematic of a gasifier stove with the gasification air flowing from bottom to top, and another stream of air through radial holes at the top helps combustion of the combustible gases; the part on the right is the modification for the current experiments to help control the air flow rates.

gasification is burned on top with secondary air to ensure complete combustion and minimum emissions. Domestic cooking requires power in the range of 3–4 kW_{th}, and this corresponds to a biomass consumption of 10–15 g/min. This requires a primary air flow rate in the range of 15–25 g/min for 100 mm diameter stove; the superficial velocity corresponding to this range is 3–6 cm/s. When the stove is loaded with biomass and is lit on top by sprinkling small amounts of liquid fuel (say, alcohol or kerosene), devolatilization of biomass leads to ignition of particles in the top-most layer. This in turn leads to similar processes in the subsequent layers of biomass particles. This flame front propagates into the fuel bed against the air stream similar to a premixed flame propagation in a tube, albeit with a heterogeneous local fuel source. The air that passes from the bottom through the bed aids flaming combustion of the biomass pieces, and the gases move upward through the hot char bed left behind by the propagating pyrolysis front. This leads to reduction reactions, and the gases that issue from the top region are fuel rich. The gas flow rate bears a constant ratio to the air flow rate (1.5 for biomass, as shown below). Typically, these gases are at about 1000 K and contain 16% CO, 12% H₂, 3% CH₄, and higher hydrocarbons of 5–6%, 12% H₂O, with the remaining being nitrogen. Secondary air from the top mixes and burns with this combustible gas, ensuring complete combustion with minimum emissions and maximum possible heat transfer to the vessel.

Flaming and Char Modes

There are two phases in the consumption of the biomass. The first phase involves the evolution of volatile gases and conversion of the biomass to char by



Figure 2 Photographs of wood char combustion (left) and pellet char combustion (right) in the stove. (Figure is provided in color online.)

the propagating pyrolysis front. This referred to as the *flaming mode*. Once the front reaches the grate, all biomass is devolatilized, and about 20% of hot char is left on the grate. The air coming in through the grate causes surface oxidation of char and generates primarily CO and CO₂ and a small amount of H₂. CO₂ so generated passes through the hot char on top and can undergo reduction with carbon to form CO. The conversion process in the char mode is also gasification until the last 5% burn time. After this, the amount of char left behind is consumed in a combustion mode, and what will be left behind finally is ash. This is referred to as the *char mode*.

Preliminary experiments at a fixed primary air flow, with wood chips of two different densities (615 kg/m³ and 800 kg/m³) and pellets (1260 kg/m³) showed that the flaming mode dynamics, quantified by fuel mass burn rate and peak bed temperature, is independent of biomass density. But the behavior of char mode showed dependence on density with particles of higher density showing higher mass burn rate and temperature. Visual observation also confirmed this fact, and the difference in the combustion intensity in char mode is clear from Figure 2. A large amount of data on practical stoves with pellets having ash content of 8–10% showed char burn rates of 3–4 g/min and when run with wood pieces showed a char burn rate of 2–3 g/min. These tests also showed that 60% of the CO emissions from the stove result from the char mode with a characteristic spike during the transition from flaming to char mode (Varunkumar et al., 2011). In the context of reducing the emissions from the stove, understanding of the char mode dynamics is crucial, and the current study is focused on addressing an unusual effect observed in the char mode.

Earlier Work

In examining the relevance of earlier work seeking explanation for the above observations, it appeared that Evans and Emmons (1977) are perhaps the only researchers who have conducted a rigorous and thorough study of the combustion of wood chars of the kind typically used in domestic applications. The study has been on a one-dimensional stagnation point flow configuration, and the measurements have included burn rate, surface temperature, and heat and mass transfer coefficients. The range of velocities is more than 5 m/s, as there is extinction below this

value. It is interesting, and perhaps remarkable, that wood chars burn in one-dimensional spherical configuration at velocities as low as a few cm/s—a fact that is long known and well established (see for instance, mukunda et al., 1984). The reason for the difference lies in the observation by Evans and Emmons (1977) that the extinction begins by a heat loss at the edges. In a spherical configuration, such an opportunity for heat loss is absent, and hence combustion occurs even in the free convective mode at effective low velocities. While they have used a model for char combustion involving kinetics, large data of char spheres in conditions of the kind contemplated therein show that the process is diffusion controlled (Dasappa et al., 1994). An examination of the experimental data with their curve-fit shows that the $p_{O_{2,w}}$ is between 1% and 5%. Instead of the curve-fit $\dot{m}'' = 25.4p_{O_{2,w}}e^{-9000/T}$ and an expression for $p_{O_{2,w}}$, the data lend itself to a simpler presentation based on the consideration of diffusion limitedness: $\dot{m}'' = 3.6 \times 10^{-6}Re^{0.5}$ and $\dot{m}'' = 4.7 \times 10^{-2}e^{-5180/T}$ with the Re based on char diameter. Issues of clear laminar-like behavior for regression dependence on the flow even though inflow is turbulent have also been brought out by the investigators and require consideration beyond this article. Experiments and modeling studies on single char spheres and packed bed have been made by Dasappa et al. (1998) and Dasappa and Paul (2001). These are related to the movement of air from the top of the particle bed downwards. Thunman and Leckner (2005) and Saastamoinen et al. (2000) have conducted studies on particle beds lit from the top with air flowing from the bottom—a configuration similar to the one considered here. Thunman and Leckner (2005) observe in their article that “... conversion rate of fixed biofuel bed, operated in counter-current mode, is not much affected by density. This is somewhat surprising since the conversion of the single particles constituting the bed could be expected to depend on their density” (p. 2940). This is simply a consequence of the surface boundary conditions in the conservation equations, which relate the mass flux from the surface to thermo-chemistry and fluid flow. Further, their studies have been conducted in a manner that does not distinguish between the char mode and flaming mode of functioning, and hence the crucial aspects uncovered in the present work are missed out in their studies. This is partly related to the difference in nature of applications: their work is related to large-scale combustor operations wherein the fuel can be continuously fed from the top, whereas in the present work, it is related to domestic stove with the bed of a fixed amount, and all the mass is expected to be consumed.

The modeling study on packed-bed of coal char particles by Cooper and Hallet (2000) makes a passing observation that char density does not affect the mass burn rate—a fact that is contradicted by the present data. Perhaps, their analysis did not focus on significant changes in the density of chars since they were concerned with coal char particles only. There are a number of modeling studies on single coal char particles [Lee et al., (1995); Makino and Law, (2009); Phuoc and Annamalai, (1999); Yu and Zhang, (2009)] on ignition and steady combustion, but restricted to small sizes, less than a few mm.

The article is organized as follows:

1. Experiments on packed bed
2. Experiments on single particles
3. Model for single particle combustion

4. A simple correlation for single particles
5. Bed operation
6. Concluding remarks

EXPERIMENTS ON PACKED BED

A model stainless steel reactor, 100 mm diameter and 130 mm deep (1.0 L volume) conforming to the dimensions of the stove was constructed. The reactor was insulated using glass wool, and a cast iron grate was used to hold the fuel. Biomass was loaded in the reactor, and the amount loaded depended on the density of the fuel. Fixed flow rate of primary air measured by calibrated rotameters was supplied from the bottom of the grate. The secondary air flow was blocked during the experiments to especially examine the gasification process. Before the grate, flow smootheners were used to ensure uniform flow across the cross-section of the reactor. The mass loss rate was measured by mounting the stove on a fine balance with 0.5 g accuracy. Gas samples extracted close to the top of the bed were analyzed using a Mairhak gas analyzer for CO, CO₂, H₂, CH₄, and O₂. Bed temperatures were measured by introducing 1 mm K-type thermocouples at specific intervals along the length of the stove. The details of the biomass used in the experiments with ultimate and proximate analysis are presented in Table 1.

Experiments were conducted at air flow rates of 15, 20, and 25 g/min with wood chips of density 615 kg/m³ and pellets of 1260 kg/m³ with ash content of 1% respectively. This is the range of flow rate in which the gasification A/F is around 1.5, and it is well known in the gasification literature that around this A/F, the calorific value of the gas obtained is the optimal (Kaupp and Goss, 1984). The superficial velocity in this range of air flow rates is 3–6 cm/s. These experiments showed that the first part of the process, namely, flaming combustion, occurred at the same

Table 1 Stove operation with different biomass; gasification air = 15, 20, 25 g/min

Item	Wood chips	Pellets
Density, kg/m ³	615	1260
Size, mm dia, mm length	12, 30–40	12, 30–40
Bulk density, kg/m ³	462	794
Proximate analysis		
Volatile content, %	69	68
Char, %	20	21
Ash content, %	1	1
Moisture content, %	10	6–10
Ultimate analysis*		
C	44.4	42.5
H	6.3	5.7
O	48.8	51.6
N	0.6	0.2
Composition of the biomass	CH _{1.7} O _{0.79} N _{0.053}	CH _{1.62} O _{0.93} N _{0.022}
Air-to-fuel (stoichiometric)	5.2	4.5
Primary air-to-fuel ratio (flaming mode)	1.5	1.5

*Moisture and ash-free basis.

Table 2 Mass burn rate and peak bed temperatures in flaming and char mode

V_p (g/min)	\dot{m}_f^* (g/min)	T_f (K)	\dot{m}_c^* (g/min)	T_c (K)
Wood				
15	10.1	1027	2	1361
20	13.3	1065	2.7	1380
25	16.7	1093	3.7	1436
Pellets				
15	10.3	1042	2.4	1408
20	13.5	1099	3.6	1502
25	16.6	1120	4.2	>1533**

V_p —primary air flow rate, f—flaming, c—char.

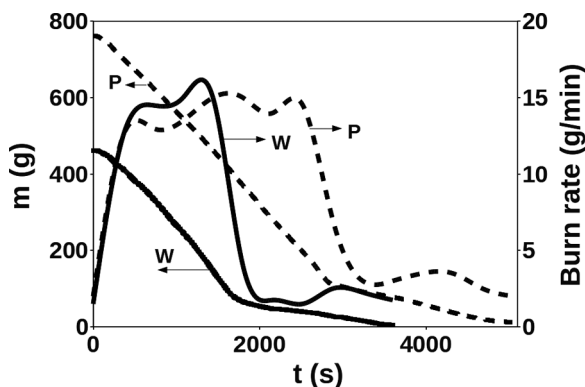
**Beyond the range of K-Type thermocouple used.

*Averaged over more than three experiments.

rate of 10, 13.3, and 16.7 ± 0.5 g/min for all biomass considered, at 15, 20, and 25 g/min air flow rate, respectively. However, the char combustion process initiated after 80–85% mass consumption showed that wood char (360 kg/m^3) burned at 2, 2.5, and 3.5 g/min, and pellet char (990 kg/m^3) burned at 2.6, 3.6, and 4 g/min, respectively, in the flow rate range chosen. An additional confirmation was obtained by using wood pieces of a higher density, 800 kg/m^3 . This exhibited a behavior for flaming mode the same as for other biomass and a char consumption rate of 2.8 g/min at 20 g/min air flow rate—a result that lies in between those of wood and pellet char. Further experiments were restricted to low-density wood and high-density pellets.

Measured values of burn rate and temperatures for wood and pellets are shown in Table 2. The data clearly show the similarity of the flaming mode and the differences in the char mode. Since the propagation is steady, the gas temperature above the bed is also steady. The data on the measured fuel mass loss, temperatures, and gas composition with burn time are presented in Figures 3–6 for 20 g/min air flow rate.

The temperature plots (see Figure 4) clearly show the propagation of the reaction front through the packed bed. The important features are marked on the plot.

**Figure 3** Mass with time for wood and pellets through the burn.

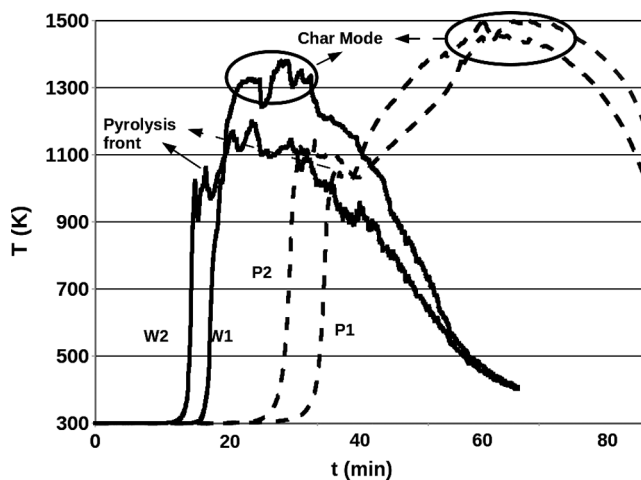


Figure 4 Bed temperature profiles. Thermocouples W1, W2 and P1, P2 refer to wood and pellets positioned 10 mm and 30 mm above the grate.

The flame front reaches the thermocouples W2 and P2 located 30 mm above the grate first at 900 and 1800s, respectively. The short peaks seen at this time are related to the location of the oxidative pyrolysis zone. The immediate dip in the profile is related to the reduction process (leading to gasification). One particular feature that needs attention is that W1 does not show a dip like other thermocouples. The flame front reaches thermocouples W1 and P1 after about 285 and 450 s, respectively, from W2 and P2. This gives a local propagation rate of 245 ± 30 and 134 ± 25 mm/h for wood and pellets, respectively. The extraction of mean values from experimental data lead to 220 and 127 mm/h respectively. The inaccuracy in local propagation measurement has been traced to particle movements in the bed close to the thermocouple. Perhaps, these issues may have led Thunman and Leckner (2005) to their

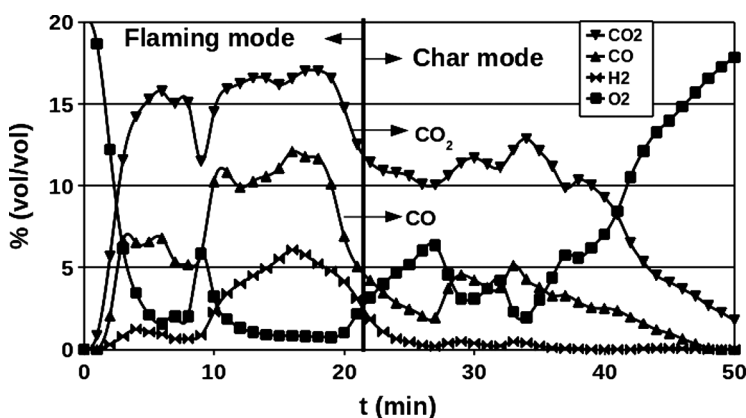


Figure 5 Composition of the gases above the packed bed of wood at 20 g/min air flow.

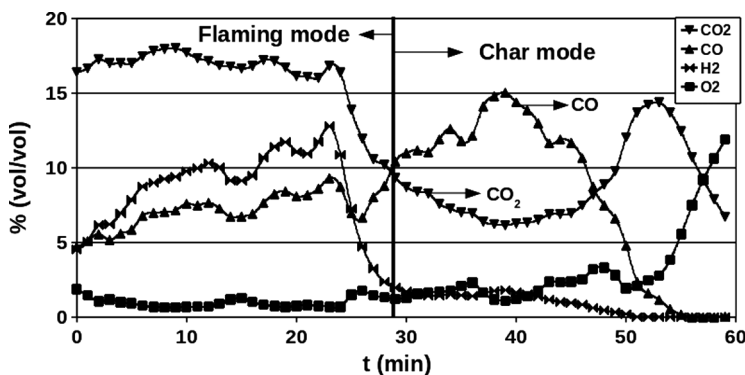


Figure 6 Composition of the gases above the packed bed of pellet at 20 g/min air flow.

results that show wide variations in air-to-fuel ratio in the gasification mode—something not found in earlier work and not easy to justify.

The expectation of constant A/F in this range of flow rates is because of the nature of gasification process. The reduction reactions have a lower temperature limit of 950–1000 K, and the amount of char consumed depends on the amount of bed that experiences temperatures above this value. Increased air flux leads to higher temperatures in the bed and hence higher rates of conversion.

Figures 5 and 6 show the gas composition measured during the operation of the reactor at 20 g/min air flow for wood and pellets. Though the flaming mode shows differences in the variation of composition between wood and pellets, char mode shows serious differences. In the char mode that begins after about 25 min for the case of wood chips and 30 min for pellets, the fraction of CO in the gas is 5–10% more in the case of pellets, and this is clearly responsible for a prominent pale blue flame on top of the pellet char bed; however, in the case of wood it is much weaker (see Figure 2). The oxygen fraction in the case of wood char increases from near 0 at the time the volatile combustion is completed to ambient mole fractions nearly linearly until the end, whereas in the case of pellet char it remains near 0 until the end. This implies that the wood chip char bed is too porous to intersect and consume all the oxygen in the air stream. Since the oxidation reactions are diffusion controlled, this result explains the difference in the char burn rates between wood and pellets.

Even though these experimental facts explain the differences between wood and pellet char beds, it is not clear whether these effects are just because of the differences in the bed properties (bed porosity and bed density) or the way that single char particles burn differently. To understand these effects, experiments were conducted on single particles under different conditions, and these are discussed in the following section.

EXPERIMENTS ON SINGLE PARTICLES

Wood spheres in the diameter range of 10–12 mm (615 kg/m^3) and pellet cylinders of diameter 8 mm and length 15 mm (1260 kg/m^3) were mounted on a fine needle and placed on a weighing balance with a precision of 1 mg. The particles were

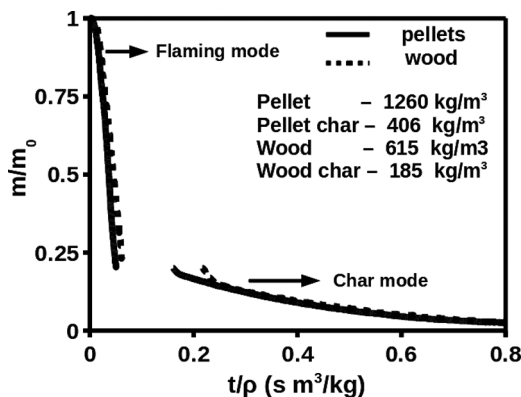


Figure 7 Mass loss with time for a wood and pellet in ambient conditions—time axis scaled with densities of corresponding particles.

ignited with a LPG flame. Wood spheres take 10–15 s to ignite and pellet cylinders about 25 s. Pellets take more time to ignite because of high thermal inertia compared to wood (see for instance, Quintiere, 2006). Mass loss with time was continuously acquired by interfacing the balance with a data acquisition system, and a typical mass loss with time plot is shown in Figure 7. Similar to a packed bed, single particles also show two distinct modes of combustion, namely flaming and char mode. Note the mass is scaled by the initial mass and burn time with densities of the particles in the corresponding modes. The break in the plot is because of the difference in densities between a virgin biomass particle and its corresponding char (see Table 3). It is clear that both pellets and wood behave the same way in flaming as well as char mode. Therefore single particle behavior in flaming and char mode is independent of particle density, and the fact that surface heat flux balance is responsible for this kind of behavior is clearly demonstrated by this simple experiment. Since the experiments focus on determining the effects of ambient temperature and stream speed on the char particles, all the particles were lit under ambient conditions (300 K) and were allowed to burn in the flaming mode under ambient conditions to ensure uniform initial conditions for the char combustion. Once all the volatiles were consumed and the particle entered the char mode, the conditions were changed appropriately by introducing streams of different velocities and temperatures. The surface and the core temperature of the particles were measured using a 100 μm R-type thermocouple by placing one pressed against the surface and one

Table 3 Volatile fraction of fuel and char properties

Item	Wood sphere	Pellet cylinder
Density, kg/m^3	615	1260
Size, mm	11.5 dia	8 dia, 15 length
Volatile fraction %	87	81
Char density, kg/m^3	185	406
Char size, mm	10 dia	7 dia, 13.7 length

at the center through a 400 μm hole. To determine the properties of the fuel and the char obtained, a few of them were quenched after the flaming mode by passing N_2 . Both wood and pellets shrink from their original dimensions. The properties are shown in Table 3. Experiments were also conducted on wood spheres of larger and smaller diameters at ambient conditions to specifically evaluate the Grashoff number effect.

It was observed that the ash layer builds up on the glowing particle and is retained throughout the burn duration. The ash layer appears porous for wood and dense for pellets, and these features are consistent with their structures; the natural cell construction in wood looses the contents and makes the structure more porous (see for instance, Dasappa et al., 1998). The pellets have no organized structure, and hence such a structural change is not obtained. This ash layer is retained in all the cases studied here. Exploring the region of stream speeds at which the ash layer is blown away showed the lower limit as 3 m/s, which is far above the velocities encountered in the stove operation.

The different conditions used and the burn times measured are shown in Table 4. The choice of low velocities is consistent with the velocities encountered by the particle in the stoves, where the velocities are small to ensure little ash particle carryover from the stove. Some experiments were made at ambient conditions with wood spheres of 6.6, 6.8, 11.5, 14.9 mm, scaled with Grashoff number as $t_b/\rho_{char} = 0.064 \times Gr^{0.25}$ where $Gr = 223 \times 10^9 d_s^3$ with t_b in s, d_s in m, ρ_{char} in kg/m^3 . For a 11.5 mm wood sphere (leading to 10 mm char sphere), the burn time is 255 s.

Seeking confirmation of the diffusion controlled behavior of char combustion, the data on char diameter for wood and equivalent diameter for pellet char are presented in Figure 8. The time is normalized with initial char density from Table 3, accounting for the differences between wood and pellet char. The variation shows a sharper drop of d^2 in the initial phase before joining the d^2 slope. This is due to

Table 4 Burn time and surface temperature of wood and pellet char particles

d_s mm	V m/s	T_0 K	t_b s	T_s K	t_b , model s
Wood spheres					
10.0	0	300	255	983 (m)	240 to 260
10.0	0.06	300	243	1003	
10.2	0.1	300	246	1005	235 to 255
10.5	0.15	300	262	1023 (m)	
9.0	0.04	400	190	1033	
9.0	0.08	400	183	1038	
9.0	0.13	400	176	1040 (m)	180 to 190
Pellet char					
10.0	0	300	556	983 (m)	
10.0	0.06	300	530	1003	
10.0	0.09	300	500	1005	
10.0	0.15	300	490	1025 (m)	
9.0	0.04	400	419	1033	
9.0	0.08	400	392	1038	
9.0	0.113	400	366	1044 (m)	

m = measured; other temperatures estimated.

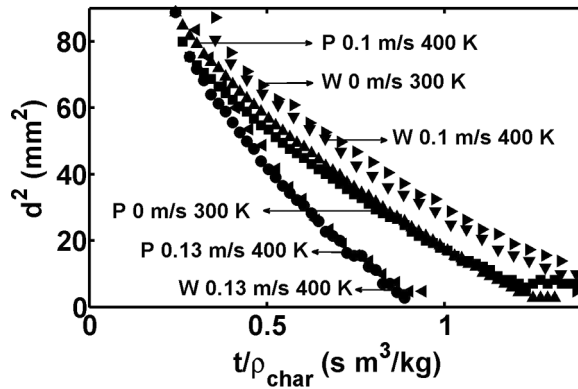


Figure 8 The variation of d^2 vs t/ρ_{char} for wood and pellet char with different air stream velocity and temperatures.

the transition from flaming to char mode. As soon as the gaseous flame extinguishes, the surface moves from 823 K to about 1050 K, at which stage there is a sharp drop to 973 K. This is a transient process, during which the ash forms on the surface; also the radiant heat loss from the surface drops sharply and settles down to a relatively slow drop rate due to increasing ash layer thickness. Beyond this transient process, the data show the linearity of d^2 vs. time behavior.

Figure 9 shows the variation of the measured surface temperature of wood and pellet chars during the burn process at ambient temperature and under quiescent conditions with time. The plot clearly shows that both the surface temperatures are the same at 973 K; the measured core temperature (not shown here) shows a similar trend with temperatures 50–60 K less than the surface temperature in the char mode. Further, the burn times shown scale with the char density. Also plotted are the outer surface temperatures corresponding to the ash layer with time. It is clear from the plot that the ash temperature drops linearly with time.

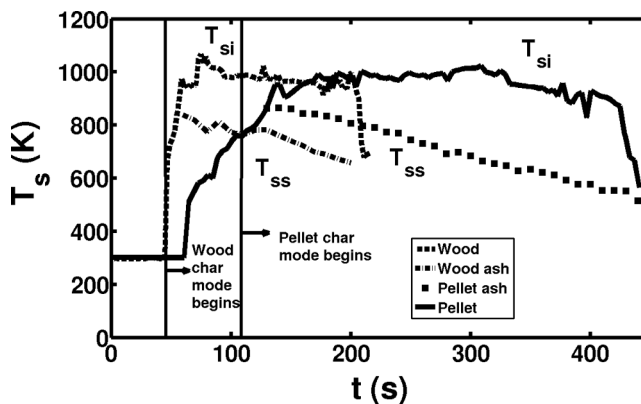


Figure 9 The variation of T_{si} , the surface temperature of the regressing char combustion surface, and T_{ss} , the surface temperature of the ash layer with time for wood and pellet chars.

MODEL FOR SINGLE PARTICLE COMBUSTION

The evolution of the model is dependent on the observation of ash buildup on wood (Glassman, 1987) and char spheres that seems to be retained largely. In this process, the surface becomes whitish with ash, such that the effective temperatures at which it radiates are much lower than the red hot surface that can be seen through the porous ash layer. In the current problem, the presence of the ash layer is imperative, as otherwise the radiant heat loss experienced at the kind of temperatures—973 K or more—is such that the char combustion cannot occur. Even if the ash layer is removed physically, the char oxidation immediately creates an ash layer, reducing the heat loss from the surface. In addition, increased ash layer thickness implies lower emissivity; both the reduced temperature and emissivity combine to make radiant heat loss small in comparison to convective heat transport. A convective balance is drawn at the surface of the ash layer. The present model does not include the few seconds when the ash layer would be forming. The heat balance at the receding surface is given by

$$\rho_{char} c_{pchar} \dot{r} (T_{si} - T_c) = \dot{q}_s'' \quad (1)$$

where \dot{r} is the surface regression rate, T_{si} is the temperature at the reaction surface that is receding, T_c is the core temperature, and \dot{q}_s'' includes the heat generated from surface reaction and the gas phase heat transfer flux due to free and forced convection at the reacting surface, as well as heat loss due to radiation. Making use of the results of the diffusion limited reaction derived from the experimental data and also supported by earlier work (Dasappa et al., 1994, 1998; Mukunda et al., 1984, 2007), it can be written as

$$\dot{q}_s'' = D\rho \frac{H}{s} \left[\frac{dY_{ox}}{dr} \right]_{r=r_{si}^+} - k \left[\frac{dT}{dr} \right]_{r=r_{si}^+} - \varepsilon\sigma(T_{ss}^4 - T_0^4) \quad (2)$$

where the first term on the right hand side is due to C-O₂ reaction, and the second term is due to conductive heat transfer at the radius $r = r_{si}$, the surface radius ($d_{si} = 2r_{si}$). The radiant loss term is based on the outer surface temperature, T_{ss} . The outer surface diameter is fixed at d_{ss} ($d_{ss} = 2r_{ss}$).

We use the idea of classical boundary layer and rewrite the results as

$$\dot{q}_s'' = D\rho \frac{H}{s} \frac{Y_{ox,0}}{\delta_{ffc} + \delta_{ash}} - \frac{k}{c_p} \frac{c_p (T_{si} - T_0)}{\delta_{ffc} + \delta_{ash}} - \varepsilon\sigma(T_{ss}^4 - T_0^4) \quad (3)$$

where H is the heat released due to C-O₂ reaction, $Y_{ox,0}$ is the free stream oxidizer fraction = 0.232 in the present experiments, δ_{ffc} is the boundary layer thickness due to free and forced convection, and δ_{ash} is the ash layer thickness. We invoke $D\rho = k/c_p$ and the transfer number B as

$$B = \frac{HY_{ox,0}}{sc_p(T_{si} - T_0)} \quad (4)$$

We can now write the flux equation as

$$\dot{q}_s'' = \frac{k}{c_p d_{ss}} (B - 1) \frac{c_p (T_{si} - T_0)}{\delta_{ffc}/d_{ss} + \delta_{ash}/d_{ss}} - \epsilon \sigma (T_{ss}^4 - T_0^4) \quad (5)$$

The balance equation can also be written as

$$\frac{\rho_{char} \dot{r} d_{ss} c_{pchar}}{k} = C_2 \frac{(T_{si} - T_0)}{(T_{si} - T_c)} \frac{(B - 1)}{\delta_{ffc}/d_{ss} + C_1 \delta_{ash}/d_{ss}} - \frac{\epsilon \sigma (T_{ss}^4 - T_0^4) d_{ss}}{k (T_{si} - T_c)} \quad (6)$$

It can be noted that the lefthand side is essentially a regression Reynolds number (we take that $\mu = k/c_p$) that is obtained from a balance of heat release, convective, and radiative fluxes. The constants C_1 and C_2 are invoked due to lack of understanding of the precise extent of thermal diffusional resistance as a function of ash thickness. They need to be chosen to fit at least one set of experimental data.

$$\frac{d_{ss}}{\delta_{ffc}} = Nu = \frac{Nu}{Nu_0} Nu_0 \quad (7)$$

Based on the earlier work Mukunda et al. (2007), the correlations can be set as

$$\frac{Nu}{Nu_0} (B - 1) = 0.7 B^{0.75} \quad \text{and} \quad Nu_0 = 2 + 0.3 Re^{0.5} + 0.7 Gr^{0.25} \quad (8)$$

The ash layer thickness is simply $\delta_{ash} = \int \dot{r} dt$. Connecting the temperature T_{ss} with T_{si} requires the solution of the conduction problem of the spherical region bounded by $r = r_{ss}$ and $r_s - \int \dot{r} dt$. While a conduction analysis with a fixed boundary temperature T_{si} at $r = r_{si}$ and a flux condition at $r = r_{ss}$ can be used to get the temperature profile, a simple relationship for T_{ss} is assumed due to uncertainties in the heat transfer processes in the porous ash layer

$$\frac{T_{si} - T_{ss}}{T_{si} - T_0} = \frac{\int_0^t \dot{r} dt}{r_{ss}} \quad (9)$$

This model has been run for several cases of wood and pellet char particles with the following data: $H = 32$ MJ/kg (assuming $C \rightarrow CO_2$, see Evans and Emmons, 1977; Scala, 2009), $s = 2.67$, $Y_{ox,0} = 0.232$, $c_p = 1000$ J/kg K, and $c_{p,char} = 700$ J/kg K. The calculated B from these and other data from earlier tables varies between 4.19 and 4.44 for various cases. The effect of transfer number can be expected to be very small. This was confirmed from specific experiments (not described here) in which single wood char spheres were burned in a furnace at temperatures from 300 to 600 K with little variation in burn time. In the model, T_{si} is set at 973 K, and T_{ss} is taken to decrease linearly with time. The emissivity is taken to reduce from 0.85 to about 0.02 exponentially in about 15 s. The results of the calculation are set out in Table 4. A range of values is shown against predictions. It was not the aim to fix the choice of parameters to get the desired result, but to examine if some chosen set of reasonable parameters will allow predictions in a reasonable range. The constants C_1 and C_2 are chosen as 15 and 0.1. A 10% change, each in C_1 and C_2 , leads to

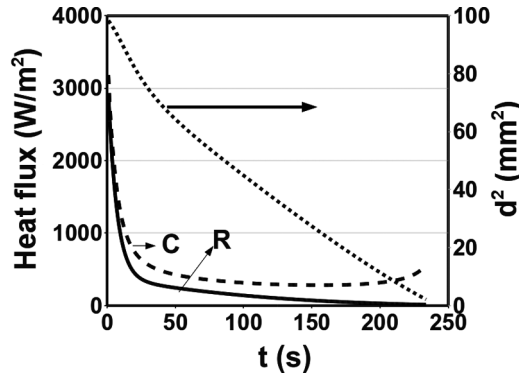


Figure 10 Convective and radiative flux in ambient conditions with d^2 variation with time.

a 9% change in burn time; 1% change in T_{ss} changes the burn time by 2.5%. Figure 10 shows the plot of various fluxes in the burn duration and the variation of d^2 with time.

The plot clearly shows two slopes for the d^2 variation with time. The initial higher slope is associated with the dynamics before the formation of the ash layer and the correspondingly high convective and radiative fluxes. The second part shows lower value for the slope and clearly indicates the role played by the ash layer in bringing down the fluxes and increasing the burn time significantly. If the dynamics of the ash layer are not included, then the wood sphere of 10 mm diameter will burn in about 27 with d^2 showing a perfect linearity with time if we neglect radiative loss. Even if the radiative loss is incorporated, without the ash layer the model will be very sensitive to chosen parameters, and burn times of the order determined in the experiments cannot be explained with such a model. Hence this model that includes the role of ash is close to realistic conditions experienced by the sphere.

A SIMPLE CORRELATION FOR SINGLE PARTICLES

Seeking a correlation of the data in terms of known scaling features was attempted. The burn time, t_b (s), scales with char density and diameter as $\rho_{char} d_s^2$, with ρ_{char} in kg/m^3 and d_s in m. It depends on the heat transfer characteristics controlled by forced and free convection. These are represented by a quantity $Re^{0.5}/Gr^{0.25}$. Figure 11 shows that the data is well correlated [Equation (10)], and the kind of scaling clearly emphasizes the fact that the phenomena are transport controlled.

$$\frac{t_b}{\rho_{char} d_s^2} = 1.38 \times 10^4 (1 - 0.19 Re^{0.5} / Gr^{0.25}) \quad (10)$$

From this set of experiments and modeling, it is clear that the single particles behave in a similar way. Therefore the explanation for higher burn rates in the char bed lies in the fact that the bed properties are different for wood and pellets.

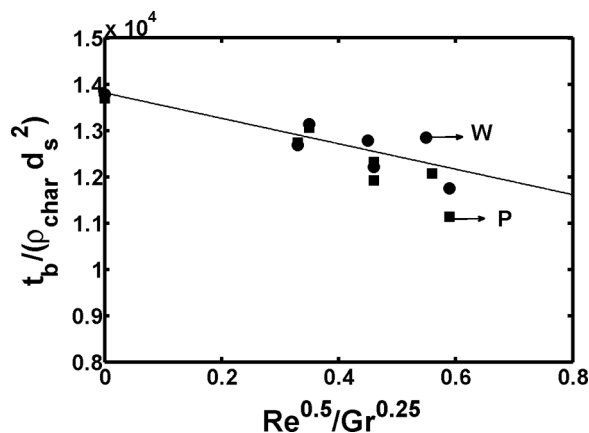


Figure 11 The normalized burn time, $t_b / (\rho_{char} d_s^2)$, with $Re^{0.5} / Gr^{0.25}$.

BED OPERATION

The bed operation is controlled by the air stream speed past the particles in the bed. Further, each particle sees other particles in close proximity, much closer in the case of pellet char than in wood char. The properties of the char bed at the time it enters into char mode of combustion are presented in Table 5. Single particles of wood and pellets under ambient conditions burn with a mass loss rate of 0.1 g/min. In a bed, the wood char consumption rate is 2.5 ± 0.5 g/min, and pellet consumption rate is 3.5 ± 0.5 g/min. Equivalent consumption in bed per particle is 0.16 g/min for wood and 0.23 g/min for pellets. Convection combined with reduced radiation loss in the bed compared to single particles is responsible for higher burn rates in the bed. Also, the heat release rate per unit combustor volume is lower for the wood char bed compared to the pellet char bed, as is evident from the fact that the packing density of pellet char bed is 38% higher than that of the wood char bed. At the same air flow rate, this difference is because closely packed pellet char particles see each other in closer proximity than wood char particles, leading to less radiation loss. This leads to higher surface temperatures (T_{si}) for pellet char compared to wood char (see Figure 4), which leads to better thermal environment for the pellet char operation. Bed temperature is an important parameter in the diffusion controlled regime here because it determines the dynamics of radiation heat transfer in the bed. The radiation loss in wood char bed is intermediate between single particle combustion and dense pellet char bed. These enable higher combustion rates in the pellet bed compared to the wood char bed.

Table 5 Char bed properties

Item	Wood char	Pellet char
Char bed depth, mm	51	76
Mass of char bed, g	55	105
Bed density, kg/m ³	110	176

Establishing the precise magnitudes calls for modeling the char bed operation, which is a subject for future study.

CONCLUDING REMARKS

Noting the significant difference in char burn rates between wood and pellet char particles in a packed bed used as a part of a domestic biomass-based stove, the work on single particles was undertaken. This has shown that mass burn rates are the same; the linear burn rates scale as the density. The regressing surface temperatures are the same. The combustion behavior obeys the d^2 law after an initial period of adjustment.

Modeling the combustion behavior of the single char particles shows that the ash layer that naturally forms on the surface during the combustion process is essential to explain the burn behavior. Experimental data on the core, regressing surface as well as the outer ash surface with time, are used as an important input for the model aimed at explaining the combustion behavior. The scaling of burn time with density and d_s^2 and the relative independence with regard to ambient temperature (B effect) are condensed into a correlation with fluid flow variables—the Reynolds and Grashoff numbers as $t_b/\rho_{char}d_s^2 = 1.38 \times 10^4(1 - 0.19Re^{0.5}/Gr^{0.25})$.

Explaining the differences of bed combustion behavior needs the observation that the bed densities are much higher for pellet char in comparison with wood char with significant heat release rate differences (of a factor of 1.6). This difference allows much higher adiabaticity in the functioning of a pellet char compared to wood char in the stove and hence the differences in the burn rates. While the modeling approach outlined here captures the combustion behavior of single char particles properly, there is still a need to extend this understanding to the combustion behavior in a bed.

NOMENCLATURE

δ_{ash}	ash layer thickness (m)
δ_{ffc}	boundary layer thickness due to free and forced convection (m)
\dot{m}''	mass burn rate per unit area ($\text{kg}/\text{m}^2 \text{ s}$)
\dot{q}''	heat flux (W/m^2)
\dot{r}	surface regression rate (m/s)
ε	emissivity
ρ_{char}	density of char (kg/m^3)
σ	Stefan–Boltzmann constant = $5.67\text{e-}8$ ($\text{W}/\text{m}^2 \text{ K}^4$)
c_p	specific heat ($\text{J}/\text{kg K}$)
Gr	Grashoff number
H	heat of reaction of carbon with air = $32 \text{ MJ}/\text{kg}$
k	thermal conductivity ($\text{W}/\text{m}^2 \text{ K}$)
Nu	Nusselt number
$p_{O_{2,w}}$	partial pressure of oxygen at the char surface (atm)
r	radius (m)
Re	Reynolds number
s	stoichiometric air-to-fuel ratio of carbon air combustion = 11.5
T_0	ambient temperature = 300 K

t_b	burn time (s)
T_c	core temperature (K)
T_{si}	burning surface temperature (K)
T_{ss}	ash surface temperature (K)
Y_{ox}	mass fraction of oxidizer

REFERENCES

- Cooper, J., and Hallet, W.L.H. 2000. A numerical model for packed-bed combustion of char particles. *Chem. Eng. Sci.*, **55**, 4551–4460.
- Dasappa, S., and Paul, P.J. 2001. Gasification of char particles in packed beds: Analysis and results. *Int. J. Energy. Res.*, **25**, 1053–1072.
- Dasappa, S., Paul, P.J., Mukunda, H.S., and Shrinivasa, U. 1994. The gasification of wood-char spheres in CO₂-N₂ mixtures: Analysis and experiments. *Chem. Eng. Sci.*, **49**, 223–232.
- Dasappa, S., Paul, P.J., Mukunda, H.S., and Shrinivasa, U. 1998. Wood-char gasification: Experiments and analysis on single particles and packed beds. *Proc. Combust. Inst.*, **27**, 1335–1342.
- Evans, D.D., and Emmons, H.W. 1977. Combustion of wood charcoal. *Fire Res.*, **1**, 57–66.
- Glassman, I. 1987. *Combustion*, 2nd ed., Academic Press, New York, Chap. 6, pp. 407–409.
- Kaupp, A., and Goss, J.R. 1984. *Small Scale Gas Producer—Engine Systems*. Vieweg, Wiesbaden, Germany.
- Lee, J.C., Yetter, R.A., and Dryer, F.L. 1995. Transient modeling of carbon particle ignition and oxidation. *Combust. Flame*, **101**, 387–398.
- Makino, A., and Law, C.K. 2009. Combustion of graphite. *Proc. Combust. Inst.*, **32**, 2067–2074.
- Mukunda, H.S., Basani, J., Shravan, H.M., and Philip, B. 2007. Smoldering combustion of “incense” sticks, experiments and modeling. *Combust. Sci. Technol.*, **179**, 1113–1129.
- Mukunda, H.S., Dasappa, S., Paul, P.J., Rajan, N.K.S., Yagnaraman, M., Ravikumar, D., and Deogaonkar, M. 2010. Gasifier stove—science, technology and out-reach. *Current Science*, **98**(5), 627–638.
- Mukunda, H.S., Paul, P.J., Shrinivasa, U., and Rajan, N.K.S. 1984. Combustion of wooden spheres. *Proc. Combust. Inst.*, **20**, 1619–1628.
- Phuoc, T.X., and Annamalai, K. 1999. A heat and mass transfer analysis of the ignition and extinction of solid char particles. *J. Heat Transfer*, **121**, 886–893.
- Quintiere, J.G. 2006. *Fundamentals of the Fire Phenomena*, John Wiley, West Sussex, England, Chap. 7, pp. 163–164.
- Saastamoinen, J.J., Taipale, R., Harttanainen, M., and Sarkomaa, P. 2000. Propagation of ignition front in beds of wood particles. *Combust. Flame*, **123**, 214–226.
- Scala, F. 2009. A new technique for the measurement of the product CO/CO₂ ratio at the surface of char particles burning in fluidized bed. *Proc. Combust. Inst.*, **32**, 2021–2027.
- Thunman, H., and Leckner, B. 2005. Influence of size and density of fuel on combustion in a packed bed. *Proc. Combust. Inst.*, **30**(2), 2939–2946.
- Varunkumar, S., Rajan, N.K.S., and Mukunda, H.S. Modern gasifier based biomass stoves: Part 2: Emissions. *Energy for Sustainable Development* (in press).
- Yu, J., and Zhang, M.C. 2009. Experimental and modeling study on char combustion. *Energy Fuels*, **23**, 2874–2885.